

---

# Graph Neural Networks are Heuristics

---

**Yimeng Min**

Department of Computer Science  
Cornell University  
Ithaca, NY, USA  
min@cs.cornell.edu

**Carla P. Gomes**

Department of Computer Science  
Cornell University  
Ithaca, NY, USA  
gomes@cs.cornell.edu

## Abstract

We demonstrate that a single training trajectory can transform a graph neural network into an unsupervised heuristic for combinatorial optimization. Focusing on the Travelling Salesman Problem, we show that encoding global structural constraints as an inductive bias enables a non-autoregressive model to generate solutions via direct forward passes, without search, supervision, or sequential decision-making. At inference time, dropout and snapshot ensembling allow a single model to act as an implicit ensemble, reducing optimality gaps through increased solution diversity. Our results establish that graph neural networks do not require supervised training nor explicit search to be effective. Instead, they can internalize global combinatorial structure and function as strong, learned heuristics. This reframes the role of learning in combinatorial optimization: from augmenting classical algorithms to directly instantiating new heuristics.

## 1 Introduction

Heuristics are the grammar of problem-solving: the means by which intelligence—human or artificial—moves from paralysis in the face of combinatorial explosion to progress through approximation. At their core, heuristics are not mere tricks or shortcuts, but strategies for reasoning under constraint, where exact solutions are unattainable or impractical.

The Travelling Salesman Problem (TSP) has long served as a proving ground for such strategies. Exact solvers like Concorde [Applegate et al., 2003] achieve optimality at exponential cost, while carefully engineered heuristics such as Lin-Kernighan-Helsgaun [Lin and Kernighan, 1973, Helsgaun, 2000] embody layers of local improvement rules that deliver state-of-the-art approximations. Simpler constructive approaches (nearest neighbor, farthest insertion) reveal the essential tradeoff between efficiency and accuracy that has always defined heuristic reasoning.

From this broader perspective, the study of TSP is part of a long tradition: the search for principled ways to navigate intractable problems through structure, approximation, and design. This stance has been formalized into algorithmic procedures that exploit structure and domain knowledge to yield good-enough solutions. Heuristics, in this view, are systematic ways of trading optimality for efficiency while still capturing the essential structure of the problem [Halim and Ismail, 2019, Christofides, 1976, Karlin et al., 2021].

We take a different view: heuristics need not be hand-crafted rules or search procedures. They can emerge directly from structure and learning. Building on the *Structure As Search* framework [Min et al., 2023, Min and Gomes, 2023, 2025], we formulate TSP as direct permutation learning. Our non-autoregressive (NAR), generative adversarial method produces Hamiltonian cycles without supervision, explicit search, or sequential decoding. The key insight is that TSP’s inherent structure—shortest Hamiltonian cycles—constrains the solution space sufficiently for neural networks to learn effective solutions through structure alone. We employ Gumbel-Sinkhorn relaxation during training

and Hungarian algorithm decoding at inference, enabling end-to-end optimization directly from the combinatorial objective.

In this sense, our method constitutes a new form of heuristic. It is not designed by hand, but arises from adversarial training dynamics and structural inductive bias. Like classical heuristics, it does not guarantee optimality; yet, like the best of them, it produces consistently strong solutions across instance sizes. Our results show that heuristics can now be *learned* rather than *engineered*, pointing toward a paradigm where structural constraints and generative models replace explicit search as the foundation of combinatorial optimization.

## 2 Background

Combinatorial optimization problems lie at the core of operations research, theoretical computer science, and many real-world decision-making systems. Classical approaches range from exact solvers, which guarantee optimality at exponential cost, to heuristic algorithms that trade optimality for scalability. Among these, greedy heuristics occupy a central role due to their simplicity, interpretability, and strong empirical performance on many structured instance families.

Graph Neural Networks (GNNs) have recently gained prominence as a tool for automating heuristic design in combinatorial optimization, moving beyond traditional manual approaches [Khalil et al., 2017, Bengio et al., 2021, Cappart et al., 2023]. Rather than hand-crafting decision rules, learning-based methods aim to infer solution strategies directly from data, leveraging structural regularities across problem instances. This paradigm has led to a wide spectrum of approaches, including reinforcement learning with autoregressive decoding, supervised learning combined with post hoc search, and unsupervised formulations that embed combinatorial constraints into differentiable objectives.

**What Does It Mean to Outperform Greedy?** Despite their conceptual appeal, the effectiveness of learning-based methods for combinatorial optimization has been the subject of sustained debate. A series of recent studies—most prominently in *Nature Machine Intelligence*—argue that modern GNN-based approaches fail to outperform classical greedy heuristics, with evidence drawn largely from evaluations on carefully chosen sparse or locally favorable regimes [Angelini and Ricci-Tersenghi, 2023, Boettcher, 2023, Schuetz et al., 2023a,b].

These findings are, in isolation, unsurprising. Greedy algorithms can be remarkably effective on instance families where global feasibility and solution quality emerge naturally from a sequence of locally sensible decisions. The deeper question, however, is not whether greedy heuristics can be strong in such regimes, but whether these evaluations capture the conditions under which learning-based methods are expected to offer a genuine advantage—or whether they instead conflate failure to outperform greedy everywhere with failure to go beyond greedy at all.

The difficulty lies in how these results are interpreted. Comparing against greedy implicitly assumes that matching or exceeding greedy performance is a reliable test of whether a model understands the problem. But greedy algorithms are local by design. They succeed precisely in regimes where local information is already sufficient. Evaluations restricted to such settings therefore blur an important distinction: whether a method is genuinely reasoning about the global structure of the problem, or merely exploiting favorable local signals.

Rather than asking whether learning-based methods can outperform greedy in regimes where greedy is expected to work well, we ask a more basic question: can they account for *global* combinatorial constraints at all? When explicit search and post hoc refinements are removed, any improvement over greedy must come from how the problem is represented and what structure the model is able to encode. In this setting, consistently outperforming a greedy baseline represents more than a marginal numerical gain; it demonstrates the model’s ability to coordinate decisions with a level of strategic foresight that surpasses local heuristics.

Seen this way, the comparison with greedy serves a diagnostic purpose. The question is not whether learning occasionally wins on favorable instances, but whether it can represent and exploit *non-local* structure that greedy algorithms, by their very construction, cannot express.

Guided by this perspective, we build a NAR learning framework designed to encode global structure. Unlike traditional autoregressive methods that construct solutions incrementally, our model predicts

a global permutation that defines the complete solution in a single forward pass. For the TSP, this approach represents tours directly as Hamiltonian cycles, enabling optimization over the manifold of permutations rather than the step-by-step assembly of paths. By embedding the Hamiltonian cycle constraint into the learning objective, the model is forced to *coordinate all decisions jointly*. Any improvement over greedy baselines in this setting must therefore arise from modeling global consistency, not from exploiting local shortcuts or post hoc refinement.

### 3 Our Contribution

We show that encoding the Hamiltonian cycle constraint of the TSP directly into the learning objective is sufficient to achieve competitive performance without reliance on search. Our method is purely unsupervised, requiring no ground-truth solutions or reinforcement rewards.

To achieve this, we introduce three elements. First, we employ an equivariant and invariant representation that preserves permutation symmetry while removing nuisance variations such as translation and rotation, ensuring that the model operates directly on the intrinsic structure of the problem. Second, we use dropout as a source of controlled stochasticity within the network, which improves robustness without introducing iterative refinement. Third, we adopt snapshot ensembling along a single training trajectory, allowing multiple functionally distinct solutions to be obtained without additional training cost.

Taken together, these elements clarify how global structure and controlled stochasticity can be incorporated into a single-pass GNN without search.

## 4 Unsupervised Learning for TSP

### 4.1 Matrix Formulation of TSP

The TSP seeks the shortest Hamiltonian cycle through  $n$  cities with coordinates  $x_i \in \mathbb{R}^{n \times 2}$ , formulated as:

$$\min_{\sigma \in S_n} \sum_{i=1}^n d(x_{\sigma(i)}, x_{\sigma(i+1)}), \quad (1)$$

where  $d(x_i, x_j) = \|x_i - x_j\|_2$  and  $\sigma(n+1) := \sigma(1)$ . We encode Hamiltonian cycles via permutation matrices. The cyclic shift matrix  $\mathbb{V} \in \{0, 1\}^{n \times n}$  is defined as:

$$\mathbb{V}_{i,j} = \begin{cases} 1 & \text{if } j \equiv (i+1) \pmod n \\ 0 & \text{otherwise} \end{cases}, \quad (2)$$

yielding:

$$\mathbb{V} = \begin{pmatrix} 0 & 1 & 0 & 0 & \cdots & 0 & 0 \\ 0 & 0 & 1 & 0 & \cdots & 0 & 0 \\ 0 & 0 & 0 & 1 & \cdots & 0 & 0 \\ \vdots & \vdots & \vdots & \vdots & \ddots & \vdots & \vdots \\ 0 & 0 & 0 & 0 & \cdots & 1 & 0 \\ 0 & 0 & 0 & 0 & \cdots & 0 & 1 \\ 1 & 0 & 0 & 0 & \cdots & 0 & 0 \end{pmatrix}. \quad (3)$$

Matrix  $\mathbb{V}$  represents the canonical cycle  $1 \rightarrow 2 \rightarrow \cdots \rightarrow n \rightarrow 1$ . Any Hamiltonian cycle matrix  $\mathcal{H} \in \mathbb{R}^{n \times n}$  is generated via similarity transformation:  $\mathcal{H} = \mathbf{P} \mathbb{V} \mathbf{P}^\top$  for permutation matrix  $\mathbf{P} \in S_n$  [Min and Gomes, 2023]. Given distance matrix  $\mathbf{D} \in \mathbb{R}^{n \times n}$ , the TSP objective becomes:

$$\min_{\mathbf{P} \in S_n} \langle \mathbf{D}, \mathbf{P} \mathbb{V} \mathbf{P}^\top \rangle, \quad (4)$$

where  $\langle \mathbf{A}, \mathbf{B} \rangle = \text{tr}(\mathbf{A}^\top \mathbf{B})$ . To enable end-to-end gradient-based optimization, we relax discrete  $\mathbf{P}$  to soft permutation  $\mathbb{T} \in \mathbb{R}^{n \times n}$ , minimizing:

$$\mathcal{L}_{\text{TSP}} = \langle \mathbf{D}, \mathbb{V} \mathbb{T} \mathbb{T}^\top \rangle. \quad (5)$$

## 4.2 From Soft Permutation $\mathbb{T}$ to Hard Permutation $\mathbf{P}$

We build the soft permutation  $\mathbb{T}$  following [Min and Gomes, 2023, 2025]. The GNN processes geometric features  $f_0 \in \mathbb{R}^{n \times 2}$  (city coordinates) and adjacency matrix:

$$A = e^{-\mathbf{D}/s}, \quad (6)$$

where  $s$  scales the distance matrix  $\mathbf{D}$ . Network output generates scaled logits:

$$\mathcal{F} = \alpha \tanh(f_{\text{GNN}}(f_0, A)), \quad (7)$$

where  $f_{\text{GNN}} : \mathbb{R}^{n \times 2} \times \mathbb{R}^{n \times n} \rightarrow \mathbb{R}^{n \times n}$  and  $\alpha$  controls scaling.

Differentiable permutation approximation via Gumbel-Sinkhorn:

$$\mathbb{T} = \text{GS} \left( \frac{\mathcal{F} + \gamma \epsilon}{\tau}, l \right), \quad (8)$$

where  $\epsilon$  denotes i.i.d. Gumbel noise,  $\gamma$  sets noise magnitude,  $\tau$  controls relaxation temperature, and  $l$  specifies Sinkhorn iterations [Mena et al., 2018].

Discrete permutation extraction at inference:

$$\mathbf{P} = \text{Hungarian} \left( -\frac{\mathcal{F} + \gamma \epsilon}{\tau} \right). \quad (9)$$

Final tour reconstruction:  $\mathbf{P} \mathbf{V} \mathbf{P}^\top$  yields the discrete Hamiltonian cycle solving the TSP instance.

Specifically, for any node reordering represented by a permutation matrix  $\pi$ , the GNN mapping satisfies

$$f_{\text{GNN}}(\pi f_0, \pi A \pi^\top) = \pi f_{\text{GNN}}(f_0, A). \quad (10)$$

As a consequence, the soft permutation  $\mathbb{T}$  produced by the Gumbel-Sinkhorn operator transforms equivariantly as  $\mathbb{T} \mapsto \pi \mathbb{T}$  under input permutations, and the corresponding heat map  $\mathbf{T} \mathbf{V} \mathbf{T}^\top$  becomes  $\pi \mathbf{T} \mathbf{V} \mathbf{T}^\top \pi^\top$ . This ensures that all node relabelings yield equivalent solutions.

## 4.3 Hamiltonian Cycle Ensemble

To mitigate long-tail failures, [Min and Gomes, 2025] employs an ensemble over Hamiltonian cycle structures  $\mathbb{V}^k$  with  $\gcd(k, n) = 1$ , where each  $\mathbb{V}^k$  encodes a distinct structural prior over tours. While effective, this design requires training a separate permutation model for each  $\mathbb{V}^k$ , as the learning objective is explicitly tied to the chosen cycle structure. Consequently, the total training cost scales with the number of coprime shifts, introducing substantial overhead compared to single-model approaches and limiting scalability to larger problem sizes.

## 5 Our Method

To avoid the cost of training multiple models, we rely on two complementary ensemble mechanisms that require only a single training run. First, we employ dropout during training and retain it at inference time, performing multiple stochastic forward passes with different dropout masks. This Monte Carlo dropout procedure yields diverse solutions from a single trained model and effectively acts as an ensemble without additional training. Second, we adopt a snapshot ensemble strategy by saving multiple checkpoints along a single training trajectory (e.g., at epochs 850, 900, 950, and 1000) and using them jointly at inference. Since all snapshots are obtained from the same optimization run, this approach introduces no extra training cost. In addition, we take a complementary architectural approach that is orthogonal to ensembling. Unlike prior work that uses raw  $x_i \in \mathbb{R}^2$  coordinates as GNN inputs, we introduce a symmetry-aware feature extraction mechanism with harmonic enhancement. This design improves representational capacity while preserving equivariance, and does not incur additional training overhead.

## 5.1 Equivariant Coordinate Feature Extraction

We introduce an *equivariant coordinate feature extractor* that maps a set of planar points to per-point features while respecting the symmetries of the Euclidean group. The construction is fully deterministic, permutation-equivariant, and (almost everywhere) invariant to global translations and rotations. The equivariant feature extraction procedure underlying these properties is illustrated in Figure 1.

### 5.1.1 Problem Setting

Let  $X = f_0 = \{x_i\}_{i=1}^n, x_i \in \mathbb{R}^2$  denote a point set. We consider group actions of: permutations  $\pi \in S_n$  acting as  $(\pi \cdot X)_i = x_{\pi(i)}$ ; translations  $t \in \mathbb{R}^2$  acting as  $(T_t \cdot X)_i = x_i + t$ ; rotations  $R \in \text{SO}(2)$  acting as  $(\mathcal{R}_R \cdot X)_i = Rx_i$ .

Our goal is to construct a feature representation that is permutation-equivariant and invariant to global translations and rotations, realized by the GNN denoted in Equation 7.

We first remove translation by centering:

$$c := \frac{1}{n} \sum_{i=1}^n x_i, \quad \tilde{x}_i := x_i - c. \quad (11)$$

We then compute the empirical covariance

$$\Sigma := \frac{1}{n} \sum_{i=1}^n \tilde{x}_i \tilde{x}_i^\top \in \mathbb{R}^{2 \times 2}. \quad (12)$$

Let  $(\lambda_1, u_\perp)$  and  $(\lambda_2, u)$  denote the eigenpairs of  $\Sigma$  with  $\lambda_1 \leq \lambda_2$ . We fix the sign ambiguity by enforcing  $u_1 \geq 0$  and apply the same sign to  $u_\perp$ , yielding a deterministic orthonormal frame

$$U := [u_\perp, u] \in \text{O}(2) := \{Q \in \mathbb{R}^{2 \times 2} \mid Q^\top Q = I\}. \quad (13)$$

This defines a *data-dependent canonical coordinate system*.

### 5.1.2 Intrinsic Coordinates and Harmonic Features

Each point is projected onto the canonical frame:

$$a_x(i) := \tilde{x}_i^\top u, \quad a_y(i) := \tilde{x}_i^\top u_\perp. \quad (14)$$

We define intrinsic polar coordinates

$$r(i) := \sqrt{a_x(i)^2 + a_y(i)^2 + \varepsilon}, \quad (15)$$

$$\theta(i) := \text{atan2}(a_y(i), a_x(i)). \quad (16)$$

Angular information is encoded using  $M$  Fourier harmonics:

$$\begin{aligned} \phi_m^{\sin}(i) &:= \sin(m \theta(i)), & m &= 1, \dots, M. \\ \phi_m^{\cos}(i) &:= \cos(m \theta(i)), \end{aligned} \quad (17)$$

The final per-point feature vector is

$$f(i) = \left[ r(i), a_x(i), a_y(i), \phi_1^{\sin}(i), \dots, \phi_M^{\sin}(i), \phi_1^{\cos}(i), \dots, \phi_M^{\cos}(i) \right]. \quad (18)$$

This feature vector is then fed into the GNN as the initial node features of the instance.

### 5.1.3 Equivariance and Invariance Properties

We now formalize the symmetry properties of the construction in Equation 7. As mentioned,  $f_{\text{GNN}}$  denotes a GNN viewed as a function that maps the initial node features to an  $n$ -dimensional output representation.

**Theorem 1** (Permutation Equivariance). *For any permutation  $\pi \in S_n$ ,*

$$f_{\text{GNN}}(\pi \cdot X, \pi A(X) \pi^\top) = \pi \cdot f_{\text{GNN}}(X, A(X)). \quad (19)$$

*Proof.* All quantities defining the canonical frame (mean, covariance, eigenvectors) are symmetric functions of the point set and invariant under reindexing. The per-point map is applied independently using this shared frame, implying equivariance. Moreover, since the adjacency matrix  $A(X)$  is constructed from pairwise distances, it transforms equivariantly under permutations as  $A(\pi \cdot X) = \pi A(X) \pi^\top$ .  $\square$

**Theorem 2** (Translation Invariance). *For any translation  $t \in \mathbb{R}^2$ ,*

$$f_{\text{GNN}}(T_t \cdot X, A(T_t \cdot X)) = f_{\text{GNN}}(X, A(X)), \quad (20)$$

*Proof.* Translation shifts the mean by  $t$  but leaves the centered coordinates  $\tilde{x}_i$  unchanged. Since pairwise distances are translation invariant, the adjacency matrix  $A = \exp(-\mathbf{D}/s)$  constructed from  $X$  is also unchanged under  $T_t$ . Consequently, the covariance, canonical frame, intrinsic coordinates, and all derived features are invariant, implying Equation 20.  $\square$

**Theorem 3** (Rotation Invariance (Almost Everywhere)). *For any rotation  $R \in \text{SO}(2)$  and any  $X$  whose covariance  $\Sigma$  has distinct eigenvalues,*

$$f_{\text{GNN}}(\mathcal{R}_R \cdot X, A(\mathcal{R}_R \cdot X)) = f_{\text{GNN}}(X, A(X)). \quad (21)$$

*Proof.* Under rotation,  $\tilde{x}'_i = R\tilde{x}_i$  and  $\Sigma' = R\Sigma R^\top$ . Thus, if  $u$  is a principal eigenvector of  $\Sigma$ , then  $Ru$  is a principal eigenvector of  $\Sigma'$ . The canonical frame therefore co-rotates with the data. Projected coordinates satisfy

$$\tilde{x}'_i^\top (Ru) = \tilde{x}_i^\top u, \quad \tilde{x}'_i^\top (Ru_\perp) = \tilde{x}_i^\top u_\perp, \quad (22)$$

implying invariance of  $(a_x, a_y)$ ,  $(r, \theta)$ , and all harmonic features. The pairwise distances are invariant under rotation; therefore, the adjacency matrix  $A = \exp(-\mathbf{D}/s)$  satisfies  $A(\mathcal{R}_R \cdot X) = A(X)$ .  $\square$

**Degenerate cases.** When  $\Sigma$  is isotropic ( $\lambda_1 = \lambda_2$ ), the principal axes are not uniquely defined; no continuous canonical orientation exists in this regime. The proposed construction is therefore invariant *almost everywhere*, which is information-theoretically optimal.

## 5.2 Dropout Regularization

**Scattering-Attention Graph Neural Network** Our model is a scattering-attention graph neural network (SCT-GNN) that combines diffusion-based representations with learnable attention-based mixing. Given node features  $X \in \mathbb{R}^{N \times d}$  and a weighted adjacency matrix  $W \in \mathbb{R}^{N \times N}$ , we first construct a set of graph operators capturing multi-scale structure [Min et al., 2022]. In particular, we use (i) normalized graph convolution operators and (ii) scattering operators derived from powers of a smoothed random-walk matrix. Each operator defines a diffusion channel that propagates information at a distinct scale.

At layer  $\ell$ , node representations are updated by aggregating diffusion features across channels:

$$H^{(\ell)} = \text{Mix}\left(\left\{\phi_k(W) H^{(\ell-1)}\right\}_{k=1}^C\right), \quad (23)$$

where  $\phi_k(\cdot)$  denotes the  $k$ -th diffusion or scattering operator, and  $C$  is the total number of channels. Rather than fixing the aggregation weights, we learn attention coefficients that adaptively combine these channels at each layer. Concretely, for node  $i$  and channel  $k$ , attention weights are computed as

$$\alpha_{i,k}^{(\ell)} = \text{softmax}_k\left(a^\top [h_i^{(\ell-1)} \parallel (\phi_k H^{(\ell-1)})_i]\right), \quad (24)$$

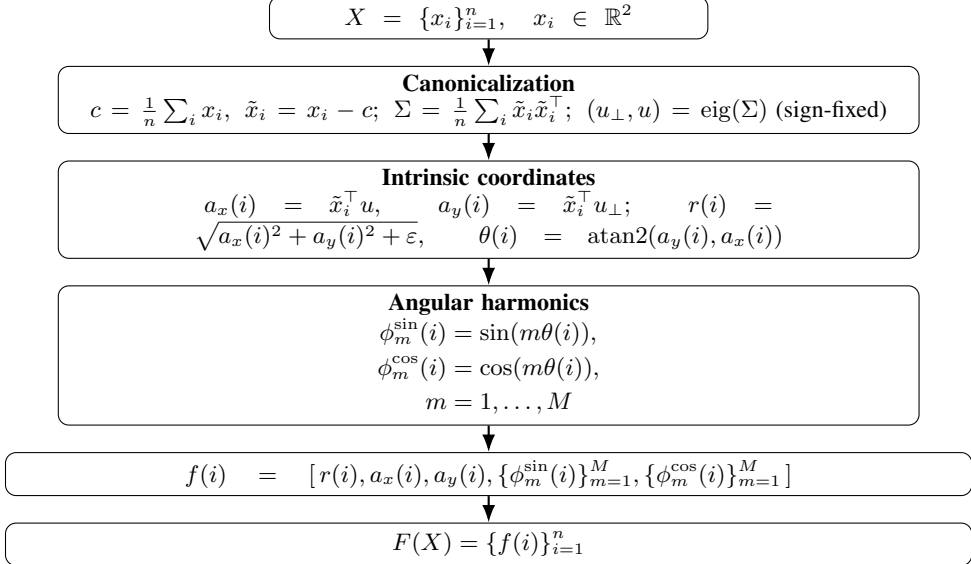


Figure 1: Illustration of the coordinate feature extractor: a canonical frame yields intrinsic polar coordinates and Fourier harmonics, concatenated into per-point features.

and the mixed representation is given by

$$\tilde{h}_i^{(\ell)} = \sum_{k=1}^C \alpha_{i,k}^{(\ell)} (\phi_k H^{(\ell-1)})_i. \quad (25)$$

The result is passed through a feed-forward transformation with residual connections, yielding the updated state  $h_i^{(\ell)}$ .

Dropout is applied within the attention weights  $\alpha_{i,k}^{(\ell)}$  and the subsequent feed-forward projections, injecting stochasticity into the feature mixing process. Importantly, this stochasticity affects only intermediate representations and does not modify the final output layer or the discrete projection used to construct tours. As a result, the model remains a single-pass heuristic, while optionally supporting stochastic inference through internal representation-level perturbations.

It should be noted that all diffusion operators and attention mechanisms are permutation-equivariant by construction, ensuring that the model respects the symmetry of the underlying graph.

**Stochastic Inference via MC Dropout.** At inference time, we optionally introduce stochasticity through Monte Carlo (MC) dropout to sample diverse solutions from a single trained model. When MC dropout is disabled, the inference procedure is deterministic: for a fixed input instance, the model produces a unique output and hence a single tour. Enabling MC dropout injects controlled randomness into the network computation, causing repeated forward passes on the same instance to yield different outputs. While the resulting perturbations are small in the continuous output space, they may lead to qualitatively different tours after the discrete projection to a permutation. MC dropout does not involve search, instead, it provides a lightweight means of generating solution diversity, allowing a trade-off between computational cost and solution diversity.

### 5.3 Snapshot Ensembles

Snapshot ensembling exploits the dynamics of a single training trajectory to obtain multiple diverse models without repeated training [Huang et al., 2017]. The key insight is that modern neural network optimization traverses a sequence of distinct regions in parameter space before convergence. Intermediate checkpoints along this trajectory can therefore serve as effective ensemble members, even though they are produced by a single optimization run.

In our setting, training GNNs entails navigating a highly non-convex loss landscape. Consequently, model parameters obtained at different epochs, including late in training, can correspond to function-

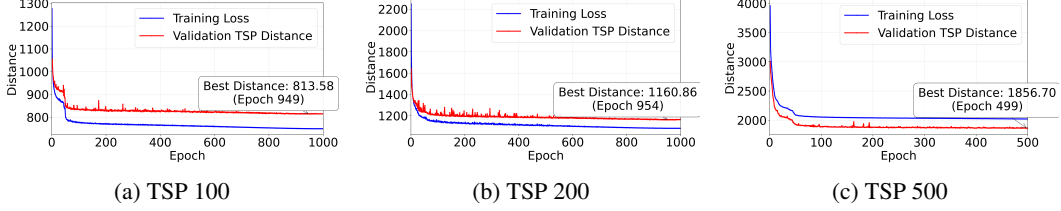


Figure 2: Training history on different sizes.

ally distinct solutions with comparable loss values but differing empirical performance. Ensembling these checkpoints reduces variance and mitigates failure modes associated with any single model instance. Importantly, this diversity emerges naturally from the optimization dynamics and requires neither explicit architectural modifications nor multiple random initializations.

In our framework, we adopt snapshot ensembling by selecting a small set of checkpoints from a single training run. Concretely, for a model trained over  $t_{\max}$  epochs, we select checkpoints at epochs

$$\{t_1, t_2, \dots, t_m\}, \quad \text{e.g., } \{850, 900, 950, 1000\},$$

or more generally by sampling snapshots at fixed intervals (e.g., every 50 epochs) during the later stages of training. Each snapshot is then used independently at inference time, and the final solution is selected or aggregated across snapshots.

In practice, we form a simple ensemble by performing multiple stochastic forward passes and selecting, for each instance, the best tour among the sampled outputs, effectively realizing an ensemble over implicit models without additional training or architectural changes. Our stochasticity arises entirely within the network forward pass and does not involve iterative refinement or neighborhood exploration. Unlike approaches used in [Min and Gomes, 2025] that require training multiple models with different structural priors, our methods shift diversity generation entirely into the training dynamics. This allows us to recover the robustness benefits of ensembling while avoiding the substantial computational overhead associated with repeated end-to-end training.

## 6 Training and Inference

We train our scattering-attention GNN using distributed data parallelism on multi-node GPU clusters. For TSP100 and TSP200, we launch runs on 2 nodes with 4 GPUs per node (8 GPUs total), using per-GPU batch size 256 and the Adam optimizer with weight decay  $2.5 \times 10^{-5}$ , dropout 0.1, and a learning rate  $8 \times 10^{-3}$ . We train for up to 1000 epochs for TSP 100 and 200, and 500 epochs for TSP 500, with a scheduler and a 15-epoch warmup, enable adaptive gradient clipping, and apply early stopping with patience 100; checkpoints are saved every 5 epochs with automatic resume enabled. For TSP500, we scale to 4 nodes with 4 GPUs per node (16 GPUs total) and train a larger model (hidden dimension 384, 48 layers) with dropout 0.5, learning rate  $2 \times 10^{-3}$ , weight decay  $10^{-4}$ , and temperature  $\tau = 3.5$ , using a smaller per-GPU batch size of 50 due to memory constraints. Across all settings, training and validation instances are sampled from uniform Euclidean TSP distributions, and we fix the distance scale to 5.0 to match the inference-time construction of the graph adjacency.

The training datasets consist of 1.5, 2.0, and 5.0 million uniformly sampled instances for TSP 100, TSP 200, and TSP 500, respectively. For each setting, we use 1,000 instances for validation and 1,000 for testing. All experiments are conducted on a compute cluster equipped with Intel Xeon Gold 6154 CPUs and NVIDIA A100 GPUs.

## 7 Results

Figure 2 shows the training history across different problem sizes. In all cases, the training objective decreases rapidly during the early stages of optimization and stabilizes as training progresses, indicating consistent convergence behavior. The validation curves closely track the training loss, with no signs of instability or divergence, suggesting that the learned representations generalize well across instances.

## 7.1 Length Distribution

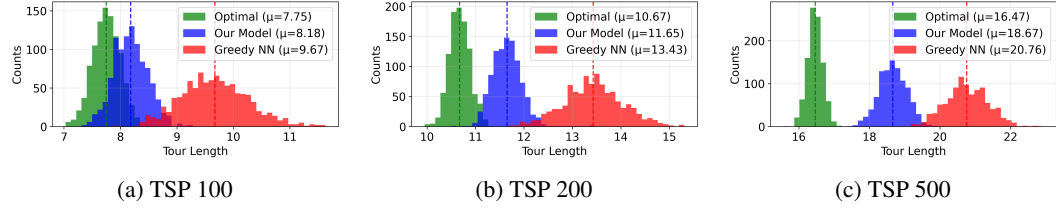


Figure 3: Comparison showing our model vs. greedy nearest neighbor baseline.

Figures 3 show the tour-length distributions on the test set for 100-, 200-, and 500-node instances, using the model that achieves the lowest validation length across all hyperparameter settings. Across all problem sizes, our method consistently outperforms the Greedy Nearest Neighbor (NN) baseline, which constructs tours by iteratively selecting the closest unvisited node. The resulting histograms show that our model produces shorter and more tightly concentrated tour-length distributions, with mean lengths of  $\mu = 8.18, 11.65$ , and  $18.84$ , compared to Greedy NN’s  $\mu = 9.67, 13.43$ , and  $20.76$ , respectively.

Table 1: Performance of a size-10 MC-dropout ensemble evaluated on Euclidean TSP instances with  $n \in \{100, 200, 500\}$ . The win rate reports the percentage of test instances for which a given run produces the shortest tour among all runs in the ensemble for the same instance.

Size	Metric	Deterministic	MC-1	MC-2	MC-3	MC-4	MC-5	MC-6	MC-7	MC-8	MC-9	Ensemble
100	Mean length	8.18	8.23	8.23	8.22	8.23	8.23	8.23	8.23	8.23	8.23	8.11
	Wins (%)	18.4	9.9	11.0	9.1	8.0	8.7	9.3	9.3	7.9	8.4	
200	Mean length	11.65	11.77	11.77	11.76	11.77	11.77	11.77	11.77	11.77	11.78	11.57
	Wins (%)	27.4	8.4	7.4	10.3	8.1	8.3	8.4	8.2	6.3	7.2	
500	Mean length	18.67	18.72	18.72	18.73	18.73	18.72	18.73	18.73	18.72	18.72	18.54
	Wins (%)	16.3	8.8	8.8	9.2	9.5	9.7	10.0	8.5	9.7	9.5	

Table 1 illustrates the behavior of our MC-dropout ensemble on Euclidean TSP instances with  $n \in \{100, 200, 500\}$ . Each column corresponds to a single inference run of the same trained model evaluated on the test set. The deterministic run (without MC dropout) consistently achieves both the lowest average tour length and the highest win rate across all problem sizes (e.g., 18.4% on TSP100), highlighting the stability of a single-pass heuristic. In contrast, individual stochastic runs yield slightly higher average tour lengths, but collectively generate a diverse set of solutions, reflecting the controlled variability introduced by MC dropout.

Table 2: Performance of a size-5 snapshot ensemble evaluated on Euclidean TSP instances with  $n \in \{100, 200, 500\}$ .

Size	Metric	Deterministic	Snapshot-1	Snapshot-2	Snapshot-3	Snapshot-4	Ensemble
100	Mean length	8.18	8.20	8.19	8.18	8.18	8.12
	Wins (%)	27.5	20.0	21.3	10.6	20.6	
200	Mean length	11.65	11.68	11.66	11.66	11.65	11.57
	Wins (%)	21.7	20.3	22.1	20.6	15.3	
500	Mean length	18.67	18.76	18.72	18.72	18.70	18.52
	Wins (%)	29.3	13.6	17.3	17.5	22.3	

Table 2 illustrates the behavior of our snapshot ensemble across problem sizes. Each column corresponds to a single inference run using the same model architecture, but taken from different training epochs. For TSP-100 and TSP-200, snapshots are drawn from training epochs  $\{850, 900, 950, 1000\}$ , while for TSP-500 they are taken from  $\{350, 400, 450, 500\}$ .

The deterministic model (equivalently, the best-validation snapshot) is consistently among the strongest single predictors, achieving the lowest average tour length for  $n = 100$ , tying for the lowest average tour length for  $n = 200$ , and remaining the strongest at  $n = 500$ . However, the snapshot that maximizes win rate is not always the best-validation one. In particular, for  $n = 200$ ,

Table 3: Performance comparison on Euclidean TSP instances with  $n \in \{100, 200, 500\}$ , where all instances are drawn from a uniform distribution in the unit square. We report average tour length, optimality gap relative to Concorde, and average runtime. All learning-based baselines are taken from [Fu et al., 2021], while classical methods are evaluated using widely adopted reference implementations. Our method is a *pure heuristic*: it constructs a complete tour in a single forward pass, without search.

Method	Type	TSP100			TSP200			TSP500		
		Length	Gap	Time	Length	Gap	Time	Length	Gap	Time
Concorde	Solver	7.75	0.00%	0.21s	10.67	0.00%	1.18s	16.47	0.00%	14.25s
GAT [Deudon et al., 2018]	RL, S	8.83	13.86%	0.29s	13.17	22.91%	2.27s	28.63	73.03%	9.46s
GAT [Kool et al., 2018]	RL, S	7.97	2.74%	0.44s	11.45	6.82%	2.10s	22.64	36.84%	7.33s
GAT [Kool et al., 2018]	RL, G	8.10	4.38%	0.01s	11.61	8.31%	0.04s	20.02	20.99%	0.71s
GAT [Kool et al., 2018]	RL, BS	7.95	2.48%	0.60s	11.38	6.14%	2.70s	19.53	18.02%	10.31s
GCN [Joshi et al., 2019]	SL, G	7.88	1.48%	0.19s	17.01	58.73%	0.46s	29.72	79.61%	3.13s
GCN [Joshi et al., 2019]	SL, BS	7.88	1.48%	0.19s	16.19	51.02%	2.17s	30.37	83.55%	17.82s
Christofides [Christofides, 1976]	Heuristic (networkx)	8.69	12.12%	0.11s	12.03	12.75%	0.58s	18.66	13.30%	6.00s
2-opt	Heuristic (C++)	8.69	12.13%	1.29s	11.92	11.72%	5.99s	18.33	11.29%	44.65s
Greedy	Heuristic (C++)	9.67	24.77%	0.04ms	13.43	25.87%	0.11ms	20.76	26.05%	0.63ms
Nearest-Neighbor										
Ours (batch size = 512) no MC dropout	GNN, UL	8.18	5.55%	0.34ms	11.65	9.18%	0.96ms	18.67	13.36%	5.84 ms
Ours (batch size = 512) snapshot ensembling: 5	GNN, UL	8.12	4.77%	1.69ms	11.57	8.83%	4.75ms	18.52	12.47%	29.19ms
Ours (batch size = 512) dropout ensembling: 10	GNN, UL	8.11	4.65%	3.37ms	11.57	8.43%	9.48ms	18.54	12.57%	59.34ms

Snapshot-2 attains the highest win rate (22.1%), exceeding that of the deterministic model (21.7%). This observation highlights that different snapshots exhibit distinct trade-offs between average solution quality and instance-wise dominance.

Although individual snapshots generally produce slightly higher average tour lengths than the deterministic model, they generate a diverse set of candidate tours. This diversity is analogous in spirit to MC-dropout ensembles, yet does not rely on injecting stochasticity at inference time. By selecting the best solution among multiple deterministic snapshots, the snapshot ensemble consistently improves the overall mean tour length across all problem sizes while preserving fully deterministic inference.

Importantly, our ensemble models exploit the diversity without introducing search or iterative refinement. These results indicate that the observed diversity arises from optimization-induced variations in the learned representations rather than explicit exploration, thereby preserving the non-iterative nature of the heuristic.

Table 3 reports the performance of our model and the compared methods. We compare against classical heuristics implemented using widely adopted and optimized reference codebases. Specifically, the Christofides heuristic is implemented using the `networkx` library, while the Greedy Nearest-Neighbor and 2-opt heuristics are implemented in optimized C++ with high efficiency. Our method is evaluated using batched inference with batch size 512 on an A100 GPU, whereas classical heuristics are executed on CPU [Hagberg and Conway, 2020].

Despite being a purely feed-forward model that constructs a complete tour in a single pass, our method reduces the optimality gap of Greedy by more than a factor of two on TSP 100 and TSP 200, and by nearly half on TSP 500. This improvement does not arise from local refinement or search, but from the model’s internalization of global TSP structure through the objective in Equation 5.

Compared to prior learning-based approaches, our method occupies a fundamentally different point in the quality-efficiency landscape. Reinforcement learning and supervised models often rely on

autoregressive decoding, beam search, or hybrid pipelines with local improvement heuristics to achieve competitive performance, incurring substantial computational overhead at inference time. In contrast, our GNN operates as a standalone heuristic: a single forward pass produces a complete solution, yet achieves solution quality that is competitive with, and in several cases superior to, stronger learning-based baselines.

Notably, many existing learning-based methods still struggle to consistently outperform simple greedy heuristics when stripped of search or post hoc refinement. By directly embedding the Hamiltonian cycle constraint into the learning objective and predicting global permutation operators.

Compared to other heuristics, the proposed method exhibits a consistently more favorable trade-off between solution quality and inference cost. As reported in Table 3, classical heuristics such as Christofides achieve optimality gaps of 12.12%, 12.75%, and 13.30% on TSP 100, 200 and 500, respectively. In contrast, our purely feed-forward GNN heuristic attains substantially lower gaps of 5.55% and 9.18% on TSP 100 and 200 in the deterministic setting, and further reduces the gap to 4.77% and 8.83% using snapshot ensembling. On TSP 500, our snapshot and MC-dropout ensembles achieve gaps of 12.47% and 12.57%, closely matching Christofides while operating at millisecond-level inference time on GPUs. Heuristics such as 2-opt reduce this gap, but at the cost of substantially higher runtime, particularly on larger instances. These results demonstrate that learned, structure-aware heuristics can match or exceed the performance of carefully engineered classical methods, while maintaining dramatically lower computational overhead.

## 8 Conclusion

We propose an unsupervised, non-autoregressive graph neural network heuristic that constructs complete TSP solutions in a single forward pass by directly encoding global combinatorial constraints into the learning objective, without reliance on search. Our performance gains arise from three elements: symmetry-aware equivariant representations that preserve permutation structure, controlled stochasticity via dropout to improve robustness, and snapshot ensembling along a single training trajectory to obtain diverse solutions at no additional training cost. Together, these elements position graph neural networks as effective heuristics for combinatorial optimization and suggest a path toward broader applicability through more expressive symmetry-aware architectures and extensions to related problems.

## 9 Acknowledgement

This project is partially supported by the Eric and Wendy Schmidt AI in Science Postdoctoral Fellowship, a Schmidt Futures program; the National Science Foundation (NSF) and the National Institute of Food and Agriculture (NIFA); the Air Force Office of Scientific Research (AFOSR); the Department of Energy; and the Toyota Research Institute (TRI).

## Ethical Statement

There are no ethical issues.

## References

Maria Chiara Angelini and Federico Ricci-Tersenghi. Modern graph neural networks do worse than classical greedy algorithms in solving combinatorial optimization problems like maximum independent set. *Nature Machine Intelligence*, 5(1):29–31, 2023.

David Applegate, Robert Bixby, Vasek Chvátal, and William Cook. Concorde tsp solver. <http://www.math.uwaterloo.ca/tsp/concorde.html>, 2003.

Yoshua Bengio, Andrea Lodi, and Antoine Prouvost. Machine learning for combinatorial optimization: a methodological tour d’horizon. *European Journal of Operational Research*, 290(2):405–421, 2021.

Stefan Boettcher. Inability of a graph neural network heuristic to outperform greedy algorithms in solving combinatorial optimization problems. *Nature Machine Intelligence*, 5(1):24–25, 2023.

Quentin Cappart, Didier Chételat, Elias B Khalil, Andrea Lodi, Christopher Morris, and Petar Veličković. Combinatorial optimization and reasoning with graph neural networks. *Journal of Machine Learning Research*, 24(130):1–61, 2023.

Nicos Christofides. Worst-case analysis of a new heuristic for the travelling salesman problem. Technical report, 1976.

Michel Deudon, Pierre Courtnut, Alexandre Lacoste, Yossiri Adulyasak, and Louis-Martin Rousseau. Learning heuristics for the tsp by policy gradient. In *Integration of Constraint Programming, Artificial Intelligence, and Operations Research: 15th International Conference, CPAIOR 2018, Delft, The Netherlands, June 26–29, 2018, Proceedings 15*, pages 170–181. Springer, 2018.

Zhang-Hua Fu, Kai-Bin Qiu, and Hongyuan Zha. Generalize a small pre-trained model to arbitrarily large tsp instances. In *Proceedings of the AAAI conference on artificial intelligence*, volume 35, pages 7474–7482, 2021.

Aric Hagberg and Drew Conway. Networkx: Network analysis with python. URL: <https://networkx.github.io>, pages 1–48, 2020.

A Hanif Halim and IJAoCMiE Ismail. Combinatorial optimization: comparison of heuristic algorithms in travelling salesman problem. *Archives of Computational Methods in Engineering*, 26(2):367–380, 2019.

Keld Helsgaun. An effective implementation of the lin–kernighan traveling salesman heuristic. *European journal of operational research*, 126(1):106–130, 2000.

Gao Huang, Yixuan Li, Geoff Pleiss, Zhuang Liu, John E Hopcroft, and Kilian Q Weinberger. Snapshot ensembles: Train 1, get m for free. In *International Conference on Learning Representations*, 2017.

Chaitanya K Joshi, Thomas Laurent, and Xavier Bresson. An efficient graph convolutional network technique for the travelling salesman problem. *arXiv preprint arXiv:1906.01227*, 2019.

Anna R Karlin, Nathan Klein, and Shayan Oveis Gharan. A (slightly) improved approximation algorithm for metric tsp. In *Proceedings of the 53rd Annual ACM SIGACT Symposium on Theory of Computing*, pages 32–45, 2021.

Elias Khalil, Hanjun Dai, Yuyu Zhang, Bistra Dilkina, and Le Song. Learning combinatorial optimization algorithms over graphs. *Advances in neural information processing systems*, 30, 2017.

Wouter Kool, Herke Van Hoof, and Max Welling. Attention, learn to solve routing problems! *arXiv preprint arXiv:1803.08475*, 2018.

Shen Lin and Brian W Kernighan. An effective heuristic algorithm for the traveling-salesman problem. *Operations research*, 21(2):498–516, 1973.

Gonzalo Mena, David Belanger, Scott Linderman, and Jasper Snoek. Learning latent permutations with gumbel-sinkhorn networks. *arXiv preprint arXiv:1802.08665*, 2018.

Yimeng Min and Carla Gomes. Unsupervised learning permutations for tsp using gumbel-sinkhorn operator. In *NeurIPS 2023 Workshop Optimal Transport and Machine Learning*, 2023.

Yimeng Min and Carla P Gomes. Structure as search: Unsupervised permutation learning for combinatorial optimization. *arXiv preprint arXiv:2507.04164*, 2025.

Yimeng Min, Frederik Wenkel, Michael Perlmutter, and Guy Wolf. Can hybrid geometric scattering networks help solve the maximum clique problem? *Advances in Neural Information Processing Systems*, 35:22713–22724, 2022.

Yimeng Min, Yiwei Bai, and Carla P Gomes. Unsupervised learning for solving the travelling salesman problem. *Advances in Neural Information Processing Systems*, 36:47264–47278, 2023.

Martin JA Schuetz, J Kyle Brubaker, and Helmut G Katzgraber. Reply to: Inability of a graph neural network heuristic to outperform greedy algorithms in solving combinatorial optimization problems. *Nature Machine Intelligence*, 5(1):26–28, 2023a.

Martin JA Schuetz, J Kyle Brubaker, and Helmut G Katzgraber. Reply to: Modern graph neural networks do worse than classical greedy algorithms in solving combinatorial optimization problems like maximum independent set. *Nature Machine Intelligence*, 5(1):32–34, 2023b.